Fast *Q*-tensor method for modeling the dynamics of defects in a liquid crystal director field

Gi-Dong Lee,[1] Philip J. Bos,[1,*] Seon Hong Ahn,[2] and Kyeong Hyeon Kim[2]
[1]*Liquid Crystal Institute, Kent State University, Kent, Ohio 44242*
[2]*AMLCD Division, Samsung Electronics, Kiheung, Kyunggi-Do, Korea*
(Received 6 December 2002; published 29 April 2003)

A fast *Q*-tensor method, which can model the defect dynamics in a liquid crystal director field, is presented. Conceptually based on the Oseen-Frank approach, we have added temperature energy density terms in addition to the strain energy terms, and an improved normalization method for fast calculations. The method is more compact and allows a larger time step than previous methods. The method is used to model the defect dynamics occurring during the topological state change from a splay to bend director field configuration.

DOI: 10.1103/PhysRevE.67.041715 PACS number(s): 61.30.Dk, 61.30.Jf

I. INTRODUCTION

Liquid crystals (LCs) have been used widely for applications including display devices and optical components for communication. In particular, recent display devices have been required to have better electro-optical characteristics such as the wide viewing angle and video rate images. Therefore, an understanding of the dynamic behavior of the LC director field has become important for the advanced LC device modes such as the π cell [1], the multidomain cell, and the PVA (patterned vertically aligned) cell [2], which can improve the electro-optical characteristics compared with conventional defect-free twisted-nematic (TN) cell. Different from the conventional TN cell, however, these types of LC modes may exhibit disclinations. In general, defects occur to allow for the transition between topologically inequivalent director configurations. One-dimensional calculations cannot give us appropriate results for modeling of the LC configurations containing defects. So, two- and three-dimensional calculations for liquid crystal cells are important for understanding the dynamics of an LC director field with defects.

In order to achieve the LC configurations in the equilibrium state, we need to calculate the minimum free energy. For the calculation of the free energy, we use the Gibb's free energy of the LC cell that is composed of elastic constants and electric field terms.

The elastic energy can be expressed with Oseen-Frank vector representation that uses three elastic constants (splay, twist, and bend) and the Landau–de Gennes *Q*-representation method [3]. The Oseen-Frank vector representation method is the more common method, but it cannot handle defects that may happen in the LC cell because it assumes that the order parameter S is a constant. As a result, it also cannot handle transitions between topologically different states (for example, splay to bend transition in the π cell). The other method, the Landau–de Gennes *Q*-tensor representation, can handle defects and topological transitions in addition to the normal dynamic behavior of LC cells by combining the thermal and strain free energy. It implies that we can achieve the information of the order parameter S in addition to LC director components n_x, n_y, and n_z. In the *Q*-tensor method, two elastic constants are yielded if we use the second-order *Q*-tensor expansion. However, it has been proved that degeneracy between splay and bend elastic constants can be removed if we use the third-order expansion [4]. Berreman has shown the relation between the Oseen-Frank elastic terms and the second- and third-order terms of the Q tensor [5]. In spite of these merits, the usual *Q*-tensor method is a complicated numerical process and requires a very small time step to prevent the divergence of the calculated results.

In a previous report [6], the defects in a π cell were modeled by using the Dickman's *Q*-tensor method. Dickman had shown that the Oseen-Frank vector representation could go directly to the *Q*-tensor representation if we use only one third-order Q component [7]. However, Dickman considered only a constant value of the order parameter S, so that the results are only qualitative in their description of defects. Previously, we have shown the fast *Q*-tensor method, which can calculate the order parameter, by adding the temperature terms in addition to the *Q*-tensor representation of the Oseen-Frank free energy terms [8]. And we have derived an improved normalization method for the faster calculations.

In this paper, we model dynamical behaviors of the LC director field with defects in a patterned-electrode π cell. The π cell is a fast response LC device that exhibits a wide viewing angle, so that it has a good potential for TV applications. However, issues with the π cell include a transition from a splay state at lower voltage to a bend state at higher voltage that involves the nucleation and motion of defects. In order to model the patterned π cell, we first review the derivation of the *Q*-tensor method, then by using the fast *Q*-tensor method, we calculate the order parameter S as well as the director components n_x, n_y, and n_z. We compare the LC director configurations from the fast *Q*-tensor method with experimental photographs.

II. NUMERICAL MODELING OF THE FAST *Q*-TENSOR METHOD

As we mentioned above, the Gibb's free energy density (f_G) consists of elastic energy density term of the LC director (f_s) and external electric free energy density term (f_e). Simply, we can achieve the total energy by integrating the calculated Gibb's free energy density. Berreman has shown

*Corresponding author. Electronic address: pbos@kent.edu

that the Landau–de Gennes Q representation for the strain energy density could be expressed as follows [5]:

$$f_s=\sum_{j=1}^{4} C_j^{(2)}G_j^{(2)}+\left[\sum_{j=1}^{4} C_j^{(3)}G_j^{(3)}+G_7^{(3)}G_7^{(3)}\right]+\cdots, \tag{1}$$

where the constants $C_j^{(n)}$ are related to elastic constants and $G_j^{(n)}$ can be defined with the values of Q tensor.

In another way, we can express elastic energy density of the LC director in the vector form. The vector form of the Frank-Oseen strain free energy density can be expressed as below:

$$\begin{aligned} f_s=&\tfrac{1}{2}K_{11}(\nabla\cdot n)^2+\tfrac{1}{2}K_{22}(n\cdot\nabla\times n)^2+\tfrac{1}{2}K_{33}(n\times\nabla\times n)^2\\ &-\tfrac{1}{2}(K_{22}+K_{24})\nabla\cdot[n(\nabla\cdot n)+n\times(\nabla\times n)]\\ &-q_0K_{22}(n\cdot\nabla\times n), \end{aligned} \tag{2}$$

where K_{11}, K_{22}, and K_{33} represent the splay, twist, and bend elastic constants, respectively. K_{24} is related to surface anchoring energy and, in the case of strong anchoring energy state, K_{24} is not needed. q_0 is the chirality of the LC.

Dickman derived the Q-tensor form of the Frank-Oseen strain free energy density:

$$\begin{aligned} f_s=&\frac{1}{12}(K_{33}-K_{11}+3K_{22})\frac{G_1^{(2)}}{S^2}+\frac{1}{2}(K_{11}-K_{22}\\ &-3K_{24})\frac{G_2^{(2)}}{S^2}+\frac{1}{2}K_{24}\frac{G_3^{(2)}}{S^2}+\frac{1}{6}(K_{33}-K_{11})\frac{G_6^{(3)}}{S^3}\\ &+q_0K_{22}\frac{G_4^{(2)}}{S^2}, \end{aligned} \tag{3}$$

$$G_1^{(2)}=Q_{jk,l}Q_{jk,l},\quad G_2^{(2)}=Q_{jk,k}Q_{jl,l},$$

$$G_3^{(2)}=Q_{jk,l}Q_{jl,k},\quad G_4^{(2)}=e_{jkl}Q_{jm}Q_{jm,l},$$

$$G_6^{(3)}=Q_{jk}Q_{lm,j}Q_{lm,k},$$

where

$$Q_{jk}=S\left(n_jn_k-\frac{\delta_{jk}}{3}\right),\quad Q_{jk,l}=\frac{\partial Q_{jk}}{\partial l}.$$

The Levi-Cività symbol e_{ijk} is 1 when subscripts are in the order of *xyz*, *yzx*, or *zxy*, and is -1 if the subscript order is *xzy*, *yxz*, or *zyx*, 0 otherwise. The δ_{jk} is the Kronecker delta, which is 1 if j equals k, and 0 otherwise.

The electric free energy density for the Q-tensor form is derived directly from $f_e=D\cdot E/2$:

$$f_e=\frac{1}{2}\varepsilon_0\left(\bar{\varepsilon}V_{,j}{}^2+\Delta\varepsilon V_{,j}V_{,k}\frac{Q_{jk}}{S}\right),$$

$$\bar{\varepsilon}=\frac{2\varepsilon_\perp+\varepsilon_\parallel}{3},\quad \Delta\varepsilon=\varepsilon_\perp-\varepsilon_\parallel,\quad V_{,j}=\frac{\partial V}{\partial j}. \tag{4}$$

By using Eqs. (3) and (4), we can calculate the LC director field from the Q tensor. In spite of this merit, this method cannot model the dynamic LC configuration including defects because it assumes a constant order parameter S that is equal to the value of S at the temperature where the elastic constants were measured.

In order to calculate order parameter S at each grid point, we need to add a temperature energy term that, in the absence of director field distortion, determines S as a function of temperature because the order parameter S is related directly to temperature. Basically, we can formulate the thermal energy density by using a simple polynomial expansion in terms of the Q tensor that is expressed as follows [3]:

$$\begin{aligned} f_i(T)=&f_0+\tfrac{1}{2}A(T)Q_{ij}Q_{ji}+\tfrac{1}{3}B(T)Q_{ij}Q_{jk}Q_{kl}+\tfrac{1}{4}C(T)\\ &\times(Q_{ij}Q_{ij})^2+O(Q^5). \end{aligned} \tag{5}$$

The restriction to a uniaxial order parameter tensor may be considered inappropriate in regions where the order parameter is spatially varying. However, it is experimentally observed that the size of the region where the order parameter is spatially varying is typically of the order of molecular dimensions. The total free energy density is the sum of Eqs. (3)–(5), so that Gibb's free energy density (f_G) can be described as the sum of these three energy densities.

In order to achieve the equilibrium state of the director configuration, it is typical to use the Euler-Lagrange equation. The following is the Euler-Lagrange equation for the electric potential and the director components under the Cartesian coordinate system. By solving Eq. (6), potential distribution and LC configurations are obtained, respectively,

$$\begin{aligned} 0&=-[f_G]_{Q_{jk}},\\ 0&=-[f_G]_V=\nabla\cdot D, \end{aligned} \tag{6}$$

where

$$[f_G]_{Q_{jk}}=\frac{\partial f_G}{\partial Q_{jk}}-\frac{d}{dx}\left(\frac{\partial f_G}{\partial Q_{jk,x}}\right)-\frac{d}{dx}\left(\frac{\partial f_G}{\partial Q_{jk,y}}\right)-\frac{d}{dx}\left(\frac{\partial f_G}{\partial Q_{jk,z}}\right),$$

$$[f_G]_V=\frac{\partial f_G}{\partial V}-\frac{d}{dx}\left(\frac{\partial f_G}{\partial V_{,x}}\right)-\frac{d}{dx}\left(\frac{\partial f_G}{\partial V_{,y}}\right)-\frac{d}{dx}\left(\frac{\partial f_G}{\partial V_{,z}}\right).$$

The terms $[f_G]_{Q_{jk}}$ and $[f_G]_V$ represent the functional derivatives with respect to the Q_{jk} and voltage V, respectively. By using these equations, we can calculate the components of the 3×3 matrix Q and voltages in each grid. For the calculation, therefore, we need to formulate functional derivative equations that are described as follows:

$$[f_G]_{Q_{jk}}=[f_G]_S+[f_G]_V+[f_G]_T, \tag{7}$$

where $[f_G]_S$, $[f_G]_V$, and $[f_G]_T$ are the strain, voltage, and temperature terms, respectively,

$$[f_G]_S = -\frac{2}{S^2}\left(-\frac{1}{12}K_{11}+\frac{1}{4}K_{22}+\frac{1}{12}K_{33}\right)Q_{jk,ll}+\frac{(K_{11}-K_{22})}{S^2}Q_{jl,lk}-\frac{K_{24}}{S^2}Q_{jl,lk}+\frac{1}{4S^3}(K_{33}-K_{11})(Q_{lm,j}Q_{lm,k}-Q_{lm,l}Q_{jk,m}$$

$$-Q_{lm}Q_{jk,ml}-Q_{lm,m}Q_{jk,l}-Q_{lm}Q_{jk,lm})+\frac{2}{S^2}q_0K_{22}e_{jlm}Q_{mk,l},$$

$$[f_G]_V = -\tfrac{1}{2}e_0D_eV_{,j}V_{,k},$$

$$[f_G]_T = \left(A_1+A_2\frac{T}{T_{ni}}\right)Q\cdot Q+A_3Q\cdot Q\cdot Q+A_4Q\cdot Q\cdot Q\cdot Q,$$

$$Q_{jk,ll} = \frac{\partial}{\partial l}\left(\frac{\partial Q_{jk}}{\partial l}\right).$$

In this equation we see an explicit dependence on S and also we know that there is an implicit dependence on S in both the K's and the Q's. At this point we will assume that the coifficents of the derivatives of Q are temperature independent. For example, in the first term we will assume that the K's are proportional to S^2, and therefore we set the value of the explicitly shown S to the value at which we assume the elastic constants were measured, (0.6). A more accurate approach accounting for the temperature dependence of the K's (and the extent of the validity of this approximation) is given by Berreman [5].

In this equation, T is the temperature, T_{ni} represents the nematic-isotropic transition temperature, and the constants from A_1 to A_4 represent the coefficients for the curve fitting polynomial. Generally, polynomial coefficients may be dependent on nematic material properties. In order to achieve the value of the coefficients, we can try to fit S as a function of temperature T to experimental data. Here, the coefficients are adjusted so that T_{ni} is at 95 °C, and so S as to be 0.6 at room temperature. As a result, the values of A_1, A_2, A_3, and A_4 as $A_1^0 = 0.79$ J/C m^3, $A_2^0 = 0.784$ J/C m^3, $A_3^0 = 0.61$ J/C m^3, and $A_4^0 = 1.474$ J/C m^3, respectively, were determined.

For the equilibrium state, the Q tensor and voltages at each grid point should be recalculated in every time step until they exhibit stable response. We can achieve this by using the dynamic equation $\gamma(\partial Q_{jk}/\partial t) = -[f_G]_{Qjk}$, where γ is rotational viscosity. To obtain an equilibrium state, we applied relaxation method based on dynamic equation for numerical calculation. As a result, the formulated relation between Q tensor of next time ${Q_{jk}}^{-\tau+1}$ and that of current time ${Q_{jk}}^{-\tau}$ is as follows:

$${Q_{jk}}^{-\tau+1} = {Q_{jk}}^{-\tau}+\frac{\Delta t}{\gamma}[f_G]_{Q_{jk}}. \tag{8}$$

Using this equation, the Q-tensor components can be updated at each time step, so that the final static value of the Q tensor is the equilibrium state. The order parameter S is related to Q tensor in the equation by $S^2 = 1.5(Q\cdot Q)$ and we can get this simultaneously with the Q components.

III. NORMALIZATION METHOD FOR TRACELESSNESS

The Landau–de Gennes Q tensor has zero trace T_r ($\Sigma Q_{ii} = 0$) and it implies that the LC director is a unit vector ($\Sigma n_i^2 = 1$). Therefore, we need to normalize the calculated new Q tensor at every time step so that it is traceless and n is a unit vector. Typically, the condition of tracelessness is directly imposed when numerically determining the equilibrium value of the Q tensor [5]. Therefore, normalizations for each time step can be achieved by the equation $Q_{ii} = (Q_{ii} - T_r/3)$. However, we have found serious problems with this method when an electric field is applied. Figure 1 shows the calculated dynamic property of a TN unit cell at 25 °C using a normalization method of tracelessness. If we apply no voltage, we can see that all of Q_{jj} components are saturated in

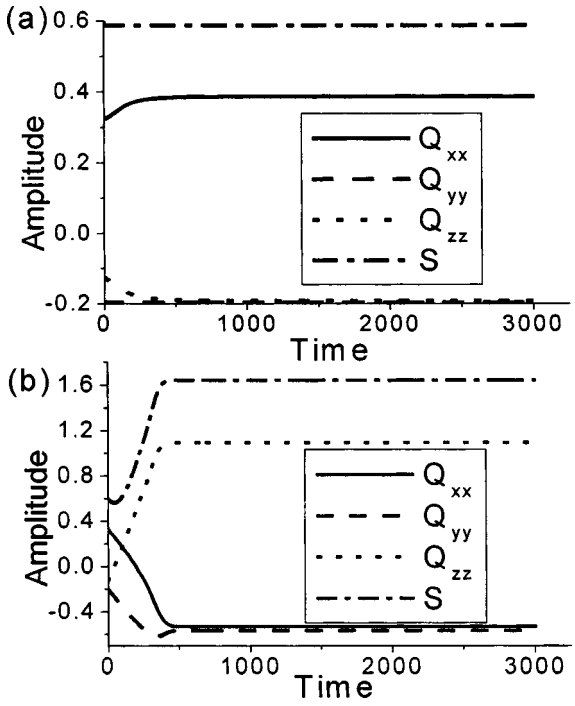

FIG. 1. Calculated dynamic behaviors of diagonal components of Q tensor and order parameter S using a normalization method based on tracelessness of the Q tensor: (a) 0 V, (b) 5 V.

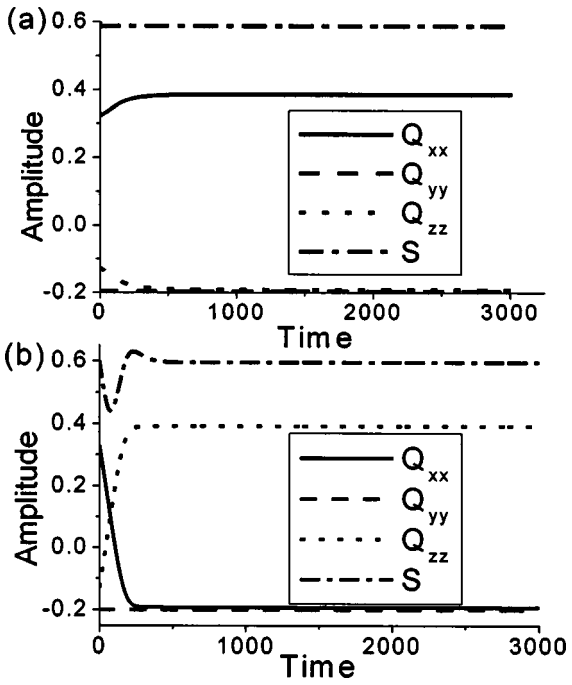

FIG. 2. Calculated dynamic behaviors of diagonal components of the Q tensor and order parameter S using a normalization method based on unitization of the LC director: (a) 0 V, (b) 5 V.

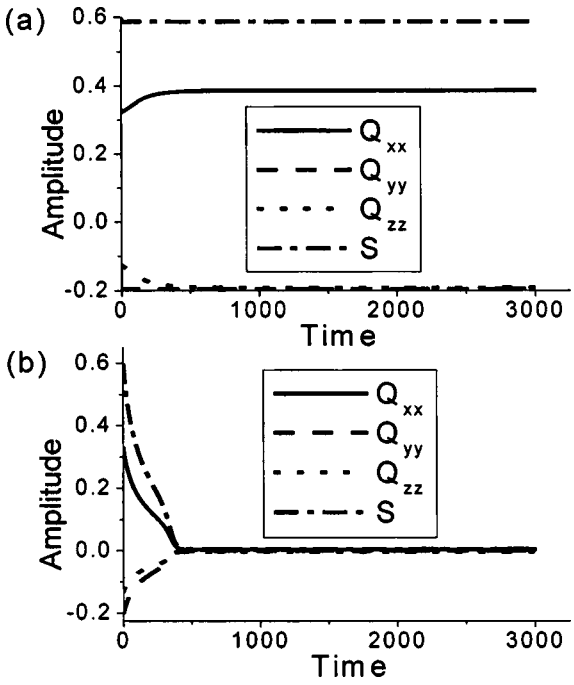

FIG. 3. Calculated dynamic behaviors of diagonal components of the Q tensor and order parameter S: (a) at room temperature (25 °C), (b) at T_{ni}.

the range from -0.2 to 0.4. However, in the case that voltage is applied, the values of Q_{jj} components deviate this range. It implies that the LC director has no longer unitized length and it does not make sense physically.

To see the cause of this condition, consider the case where the director is at 45° in the *x*-*z* plane, and a high voltage is applied along the *z* direction. The voltage term in the update equations will cause Q_{zz} to grow without bound. Only the normalization condition restrains Q_{zz} because the value of the trace will become larger than 0 at each time step. We expect that the effect of the voltage should not affect the value of Q_{yy} that should stay fixed at $-S/3$. [Recall the definition of the Q tensor: $Q_{ii}=S(n_i^2-1/3)$.] However, with the above normalization it is clear that Q_{yy} will be pushed to be more negative than $-S/3$. This condition is nonphysical and causes the calculation to become unstable. The only way to avoid very nonphysical situations is to take very small update steps.

The physical basis for the Q tensor being traceless is the fact that the director is a unit vector, and we considered that it might be more appropriate to rely on the renormalization of n directly. Writing $n_i=n_i/(|n|)$, where $|n|=(n_x^2+n_y^2+n_z^2)^{0.5}$, in terms of Q_{ii}, using the definition of Q_{ii}, we can find an improved normalization condition: $Q_{ii}=(Q_{ii}-T_r/3)$ $[S/(T_r+S)]$. It can be seen that $Q_{xx}+Q_{yy}+Q_{zz}=0$ so that the above condition causes the Q tensor to be traceless. It is also noted that the new normalization condition is simply the old one multiplied by the factor: $S/(T_r+S)$.

Returning to our example, where the director is at 45° in the *x*-*z* plane and a high voltage is applied along the *z* direction, it can be seen that the new normalization condition will never push Q_{yy} to the nonphysical condition of being more negative than $-S/3$.

Figure 2 shows the calculated dynamic property using improved normalization method. Here, stable dynamic properties are shown even with voltage applied.

IV. TEMPERATURE DEPENDENCY OF THE FAST *Q*-TENSOR METHOD

Figure 3 shows the calculated relaxation of order parameter S and the diagonal components of Q at room temperature and near the isotropic-nematic transition temperature. For this graph, it was assumed that the cell was rubbed in the plus and minus y direction and was 5 μm thick. As mentioned above, polynomial coefficients A_1-A_4 have been adjusted such that T_{ni} are around 95 °C, so that we can see order parameter S and all diagonalized Q components go to 0 at T_{ni} from a typical value of the room temperature (25 °C). Figure 4 shows more precise temperature characteristics of an order parameter S when we apply a voltage to the cell. It can be seen that by adjusting the coefficient A_1 to A_4, which gives the ratio of the coefficients of the temperature terms to the other terms in the free energy equation, the effect of a voltage on the phase transition temperature can be adjusted to meet an experimental result.

V. MODELING FOR LC DYNAMICAL BEHAVIORS OF A PATTERNED π CELL

As mentioned before, the π cell has a good potential for device applications because of its properties of fast response and wide viewing angle. In general, the director configura-

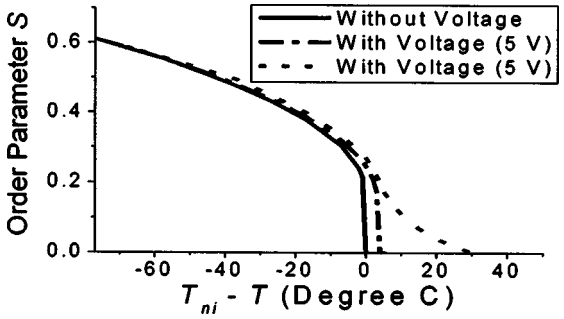

FIG. 4. The calculated dependence of the order parameter S on temperature T. The solid line represents results when no voltage is applied, the dash-dotted line and the dotted line represent the calculated results when we apply the 5 V. For the dotted lines, the values of A_1–A_4 have been changed to 0.01 times the values used for the other two curves (A_1^0–A_4^0).

tion of the π cell at 0 V is the splay state. As we apply a voltage, the director configuration goes to the bend state from the splay state. Since the derived optical switching is between the bend states, it is always necessary to apply an initial voltage to make the LC configuration transition from the splay to the bend state. Defects will necessarily be associated with the transition between the topologically inequivalent splay and bend states. In addition, the patterned-electrode cell applies a nonuniform electric field to the director field, which will affect the nucleation of defects.

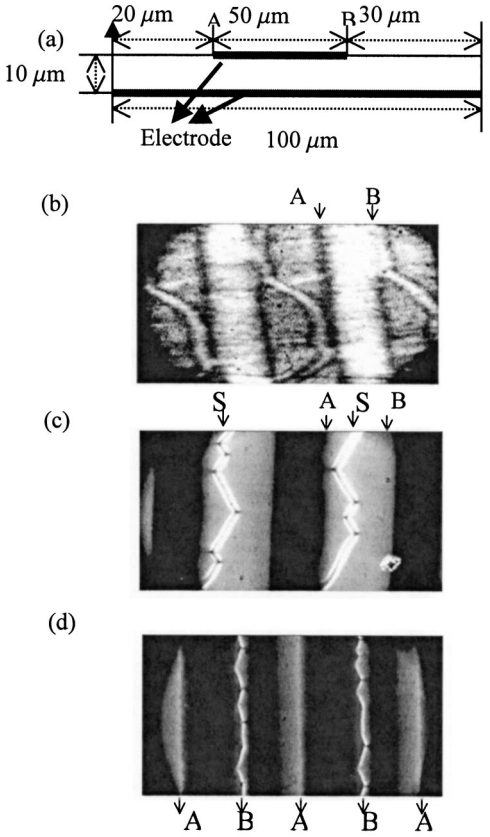

FIG. 5. The geometry of the π cell and its microphotographs: (a) a simulated structure, (b) at 2 V, (c) at 4 V, (d) at 6 V.

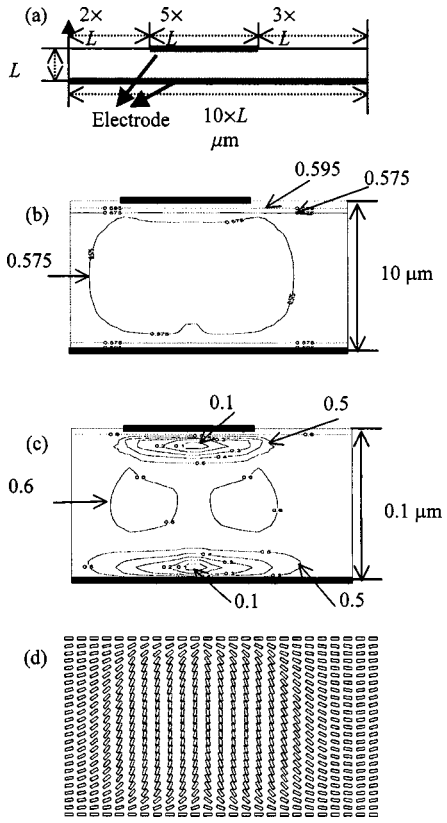

FIG. 6. The dependency of the order parameter S on the grid size: (a) a simulated structure, (b) the order parameter S with A_1–A_4=A_1^0–A_4^0, L is 10 μm and 3 V. Each line represents equi-S line in the range of 0.575–0.595. (c) The order parameter S with which L is 0.1 μm and 1.6 V. Each line represents equi-S line in the range of 0.1–0.6 with 0.1 order parameter step value. There were 50×50 grid points in the z-x plane, of which half are shown in (d).

Therefore, in order to improve the electro-optical characteristics, it is very important to model director configurations with defects in the patterned π cell.

For the experimental observation, we prepared a two-dimensional periodic patterned π cell for the experiment. Figure 5(a) shows the geometry of the π cell for the calculation. The LC material used here is *ZLI*-1565 where K_{11} is 14.4 pN, K_{22} is 6.9 pN, K_{33} is 10.7 pN, $\varepsilon_{\parallel}$ is 10.7, $\varepsilon_{\perp}$ is 3.7, q_0 is 0, and the cell gap is 10 μm. Figures 5(b)–5(d) show photographs of the cell. Here, crossed polarizers are used for the observation. Figure 5(b) shows the photograph when lower voltage that is less than the transition voltage is applied. The LC directors which are inside the electrode begin to tilt toward the z direction, so that we can recognize the variation of the retardation of the cell. As we apply the higher voltage, a defect S is observed. Figure 5(c) shows the generation of the defect in the π cell. If we apply higher voltage than Fig. 5(c), we can observe the movement of the defect to the edge of the electrode. The movement direction is dependent on rubbing direction. Figure 5(d) shows the moved defect in the patterned π cell.

In considering to proceed with the calculations, we expect from experimental observations that the spatial region where the order parameter varies from its bulk value will be quite

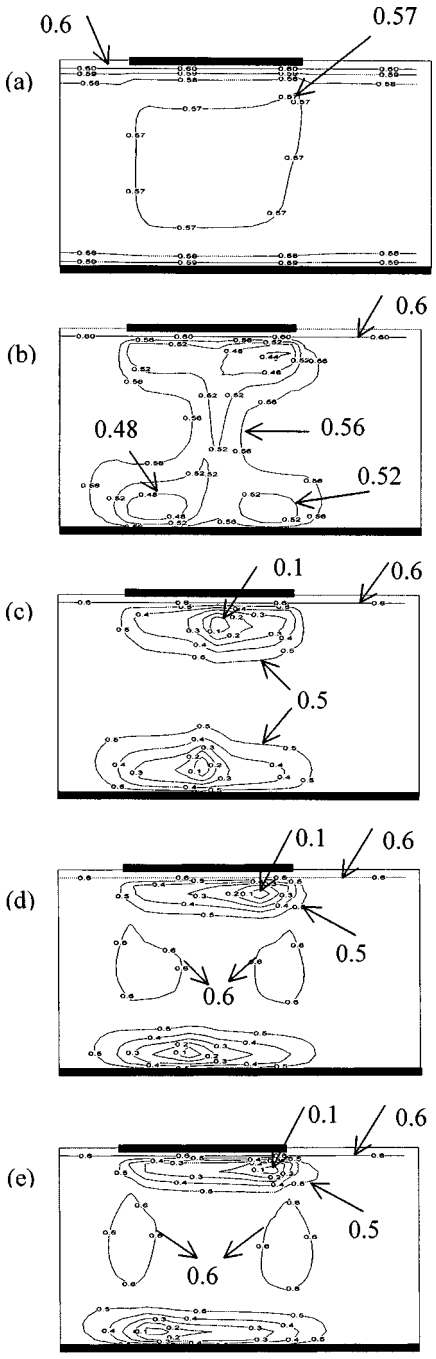

FIG. 7. The calculated order parameter S in the π cell: (a) at 0 V, (b) at 2 V, (c) at 4 V, (d) at 5 V, (e) at 6 V. $A_1-A_4=0.01(A_1^0-A_4^0)$ and the normal grid points were 50×50. Each line represents equi-S line.

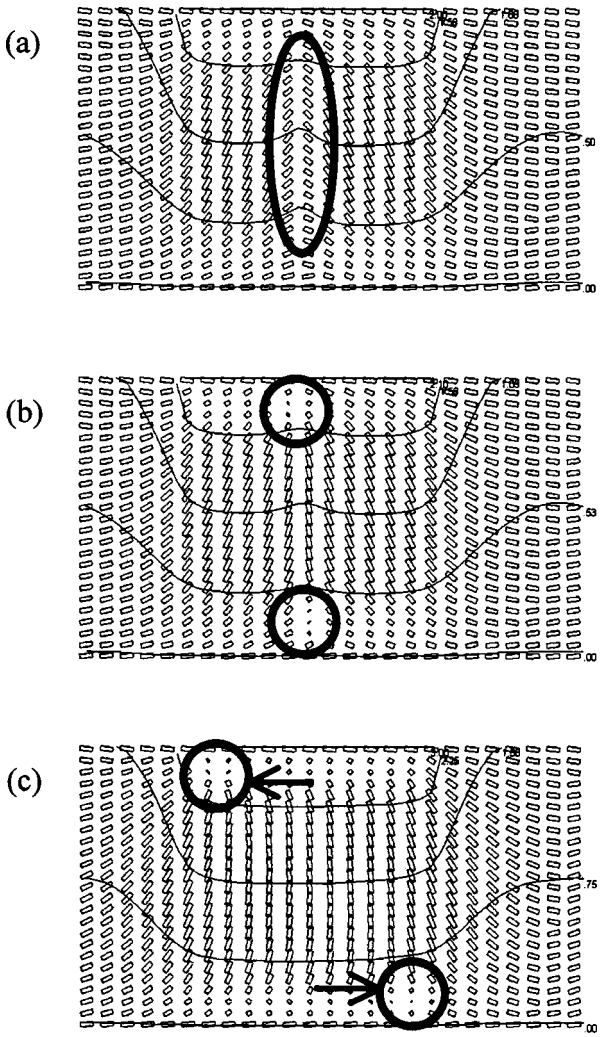

FIG. 8. Two-dimensional director calculations for the modeling of the π cell: (a) at 2 V, (b) at 4 V, (c) at 6 V under the same condition as Fig. 7. The director orientation is shown for half of the calculated grid points. The orientation of the cylinders gives the local director orientation, while their length is proportional to the order parameter S (the directors all lie in the plane of the figure). The solid lines represent equipotential lines. The electric field direction is normal to the equipotential line. The oval in (a) highlights the high elastic strain region where the pair of defects could nucleate for the case of a low anchoring energy. The circles in (b) highlight the line disclinations after they separated and moved toward the cell surfaces. The circles in (b) highlight the moved line disclination to each edge of the electrodes.

small, possibly of the order of molecular dimensions. This means that for the real system to be modeled accurately, we will need to have grid points in the vicinity of a defect spaced at approximate molecular dimensions. To be able to model a pixel that is 10 μm wide and in a cell that has a 10-μm cell gap would require $\approx1\times10^6$ grid points if a uniform grid spacing is used. If a smaller number of grid points is used we expect that deformed regions of the director field can ''disappear'' between grid points [7] before the elastic distortion energy has reached the point of causing the order parameter to decrease from its bulk value. As a result, if we consider a 10-μm pixel size with a reasonable number of grid points, we will be unable to see variations in the value of the order parameter. Figure 6 demonstrates this point. In this case we have considered a device that has a patterned electrode and a pretilt angle of zero. With this geometry, if we start with 0 V applied between the top and bottom electrodes, and increase it, we expect to see the formation of a reverse-tilt wall, followed by the formation of a pair of disclination lines ($m=\pm\frac{1}{2}$) as described by Bouligrand [3]. If

we model 50×50 grid points, we cannot see a variation in the order parameter like in Fig. 6(b) if a 10-μm cell is considered, but it is possible if the cell thickness is reduced to 0.1 μm [Fig. 6(c)], as in this case the grid point spacing is reduced to be of the order of the molecular size (the region of distortion cannot ''slip between grid points'' and the local elastic distortion energy increases to the point of causing a lowering in the order parameter). Figure 6(c) shows that with the values of A_1-A_4 equal to $A_1^0-A_4^0$, the spatial size of the region of variation in the value of the order parameter is what was expected. However, if we consider the cell thickness of our experimental cell, we are not able to consider grid points spaced as tightly as in Fig. 6(c). Therefore we will reduce the values of A_1-A_4 to be 0.01, the values found for $A_1^0-A_4^0$. In this case the defect nucleation and motion are expected to be similar to those which would be observed, but the region of defect size will be much larger (a factor of $\approx$100) than could actually occur.

Figure 7 shows the change of the order parameter S in the patterned π cell of Fig. 5 as the applied voltage is changed. We assumed hard anchoring energy at the surface of the cell, so that the order parameter S at the surface is always higher than in the bulk of the cell. Figure 7(b) shows the variation of the order parameter S at 2 V. On the center of the electrode, a wall is formed. In Fig. 7(c), we can confirm that a pair of defects is generated on the surface of the electrode. The order parameter S of those positions is reduced by around 0 and it implies that topologically inequivalent phase transition between splay and bend begins at the center point in the electrode. In terms of these phenomena, de Gennes predicted the transition of a reverse-tilt wall to a pair of disclination lines. Higher voltage makes the pair of defect move to the edge of the electrode like Figs. 7(d) and 7(e). This movement is exactly coincident with the physical phenomenon in Fig. 5(c).

Figure 8 shows the calculated director configuration of the patterned π cell in Fig. 5. In this figure the length of the cylinders is proportional to the amplitude of S, and the orientation of the cylinders gives the director orientation. From the figures, we can understand the generation of the defect pair. If the anchoring energy was very low, the defect pair would be expected to form from the region of high elastic distortion in center of the cell [the outlined area in Fig. 8(a)]. After nucleation, the movement of the pair of defects toward opposite surfaces will lower the elastic energy of the cell. However if the anchoring energy is high (as in this case), the defects appear to nucleate directly on the surfaces. After the defects have formed on the electrodes, it is clear that the movement in opposite directions along their respective surfaces further lowers the elastic energy contained in the cell. This process is consistent with the experiments and shows the dynamical behaviors in the π cell.

VI. CONCLUSIONS

The dynamical behavior of the patterned π cell by using a fast *Q*-tensor method has been discussed. It allows us to understand the generation of the defects in the cell as well as normal LC dynamical properties. We showed that a nonuniform potential distribution caused a reverse-tilt wall over a patterned electrode, so that a pair of defects formed and separated. The defects moved to lower energy state of the electrode edge finally. The calculated results explain well the experimental behavior including defects. We expect a further increase in accuracy of these results if we consider soft anchoring energy of the surface and surface morphology effects.

ACKNOWLEDGMENTS

This work was supported in part by Samsung Electronics and Korea Science and Engineering Foundation (KOSEF). The authors would like to thank Dwight Berreman for helpful discussions concerning the *Q*-tensor method.

[1] P. L. Bos and J. A. Rahman, SID '93 Digest 273 (1993).
[2] K. H. Kim and J. H. Souk, Euro Display **99**, 115 (1999).
[3] P. G. de Gennes and J. Prost, *The Physics of Liquid Crystals*, 2nd ed. (Clarendon Press, Oxford, 1993).
[4] Schiele and S. Trimper, Phys. Status Solidi B **118**, 267 (1983).
[5] D. W. Berreman and S. Meiboom, Phys. Rev. A **30**, 1955 (1984).
[6] H. Mori, E. C. Gartland, Jr., J. R. Kelly, and P. J. Bos, Jpn. J. Appl. Phys., Part 1 **38**, 135 (1999).
[7] S. Dickman, J. Eschler, O. Cossalter, and D. A. Mlynski, SID '93 Digest 638 (1993).
[8] G.-D. Lee, J. Anderson, and P. J. Bos, Appl. Phys. Lett. **81**, 3951 (2002).